

Modeling chromatic contrast sensitivity across different background colors and luminance

Marcel Lucassen¹, Dragan Sekulovski¹, Marc Lambooi¹, Qiang Xu², Ronnier Luo²;
¹Signify Research; Eindhoven, The Netherlands, ²Zhejiang University, Zhejiang, China

Abstract

In this research we compare chromatic contrast sensitivity models for two separate datasets and for the pooled dataset. They were obtained from two studies employing a very similar experimental paradigm. The data represent threshold visibilities of chromatic Gabor patterns varying in spatial frequency, background chromaticity, direction of color modulation and luminance, at constant stimulus size. Using the extended data set, we reconfirm our previously reported finding that a model based on color-opponent contrast signals is an improvement over a cone contrast model. However, when linear background scaling in classic cone contrast is replaced by nonlinear background scaling, an improvement of almost similar size is obtained. The results of this study can be of interest for the development of vision models employing the processing of spatio-chromatic information.

Introduction

The work described in this paper is a follow-up on earlier work relating to the modeling of chromatic visibility threshold data. Such thresholds are typically measured using basic visual stimuli (Gabors) featuring differences in spatial frequency and color modulation to a homogenous background. Our line of research started by the study of Vogels & Lambooi [1] who measured chromatic visibility thresholds on three background colors (located near the black body locus) at fixed luminance. The spatial frequencies employed in that study extended to the lower end because of its relevance for lighting applications where the visibility of color non-uniformities (i.e. low spatial frequencies) is undesired. In the modeling of that dataset, Lucassen *et al.* [2] found that the visibility thresholds are best described by a model incorporating opponent-like chromatic contrast signals. Since this requires the processing of signals at a stage beyond the cone photoreceptors, the model was termed the post-receptoral contrast model. Recently Mantiuk *et al.* [3] specifically tested the performance of such a model against the conventional cone contrast model on the combined data from 5 independent datasets. They found comparable performance for the two model types, but only when using mean luminance (instead of the chromatic signal itself) as normalizing factor in the post-receptoral model, otherwise the data fits with the post-receptoral model were much worse. Among the 5 datasets was

the one of Xu *et al.* [4,5], which in essence is an extension of the Vogels & Lambooi [1] dataset. It was obtained using the same methodology, employing another five background chromaticities and luminance levels. Given the high similarity in methodology for these two studies, we here take a closer look at the Vogels & Lambooi [1] and Xu *et al.* [4] datasets. For the separate and pooled datasets, we reconfirm our earlier result that post-receptoral contrast gives better data descriptions than cone contrast. Interestingly, we also show that the two model approaches only differ in the way that they normalize cone increments. When linear scaling by the background (as is done in the conventional cone contrast model) is made nonlinear, almost the same performance level as that of the post-receptoral model is reached.

Summary of experimental conditions

The data used in this paper was obtained in two separate experiments that shared the same methodology. The experimental set-up is described in detail elsewhere [1,2,5], here we only give a summary. Observers viewed an LCD monitor (NEC MultiSync, 10-bits per primary, 2560x1440 pixels) on which chromatic Gabor patterns on a homogenous background color of the same luminance were displayed. These Gabors are gratings with a sinewave color modulation, spatially blended into the background with a Gaussian envelope (see Fig. 1 for an example). The patterns varied in spatial frequency and the direction of color modulation with respect to the background. Stimulus size was fixed, implying that when varying spatial frequency, also the number of visible cycles covaried. The patterns were oriented either horizontally or vertically. While adapted to the background color, observers indicated the perceived orientation. A staircase procedure was used to control the chromatic contrast of the patterns and allowed measurement of the 75% correct detection threshold. There are two main differences between the experiments. One is the viewing distance, which was 0.5 m for the Xu *et al.* [4] experiment, and 1 m for the Vogels & Lambooi [1] experiment. The other was the background luminance, which varied for the Xu *et al.* [4] experiment, while in the Vogels & Lambooi [1] study it was fixed. Table 1 summarizes the experimental conditions.

Table 1: Experimental conditions underlying the two data sets.

Data set	adapting background	u'	v'	Y (cd/m ²)	observers	spatial frequencies	color directions
Vogels & Lambooi [1]	white 2600 K	0.2670	0.5319	108	18	6	4
	white 3800 K	0.2291	0.5106	108	18	6	4
	white 5700 K	0.2035	0.4796	108	18	6	4
Xu <i>et al.</i> [4]	white 6500 K	0.1978	0.4695	72	20	7	6
	green	0.1449	0.4758	24	19	7	6
	red	0.3155	0.5016	14.1	17	7	6
	blue	0.1700	0.3772	8.8	20	7	6
	yellow	0.2109	0.5234	50	20	7	6



Figure 1: Stimulus example at high contrast for the 5700 K background in the Vogels & Lambooij [1] study. Observers had to indicate perceived orientation of the stimulus which could be either horizontal or vertical.

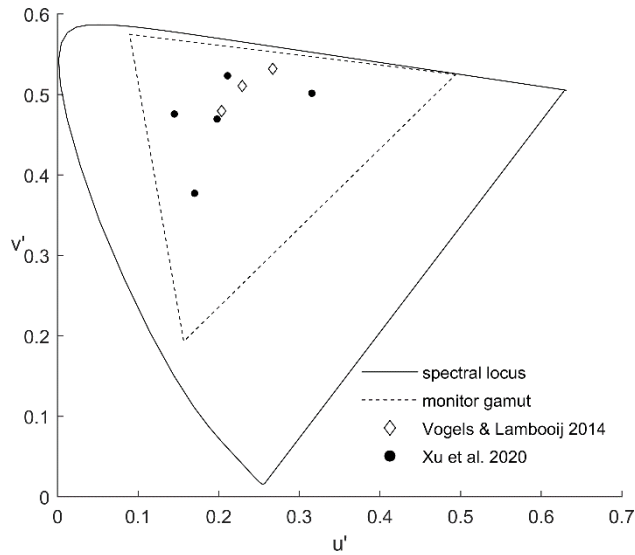


Figure 2: Color centers (adapting backgrounds) in the CIE 1976 $u'v'$ color space. The dashed triangle indicates the color gamut for the LCD monitors used in the experiments.

Data modelling

Following our earlier work [2], from the cone excitations of the background and the Gabor threshold increment we compute a detection signal from probability summation of weighted contrast signals in chromatic channels (eq.1). Since we are dealing with stimuli at isoluminance, an achromatic channel is omitted here from the usual three, leaving two chromatic channels to contribute to the detection signal:

$$signal = (|\Delta_B S_B(f)|^p + |\Delta_C S_C(f)|^p)^{\frac{1}{p}} \quad (1)$$

where Δ and S denote contrast and sensitivity, respectively, with subscript B or C for the two chromatic channels¹, f is spatial frequency and p the coefficient in Minkowski summation. In words,

¹In our previous work we defined three channels with arbitrary symbols A,B,C. A was reserved for the achromatic channel, leaving B and C for the two chromatic channels.

the contrast signals are multiplied by a frequency-dependent sensitivity factor, the absolute value of the products is raised to power p , summed, and raised to the power $1/p$. For $p=2$, eq.(1) represents a Euclidian distance. The higher the value of p , the more the detection signal is dominated by the largest of the two contributing components.

As in the previous papers, two contrast models are studied, the cone contrast model and the post-receptoral contrast model. They differ in the stage at which the contrast signals are calculated, either at the cone receptor level or at a post-receptor level (i.e. after recombination of the receptor signals). The values of the L,M,S cone excitations that appear in the equations hereafter were obtained by converting the CIE 1931 XYZ color specifications according to

$$\begin{pmatrix} L \\ M \\ S \end{pmatrix} = \begin{pmatrix} 0.34687 & 1.07301 & -0.04871 \\ -0.59010 & 1.80232 & 0.15324 \\ 0.02061 & -0.04607 & 1.32477 \end{pmatrix} \begin{pmatrix} X \\ Y \\ Z \end{pmatrix} \quad (2)$$

which was derived for the NEC display [2].

Cone contrast

The cone contrast model converts Weber-like contrast signals within each cone type into contrast signals in two chromatic channels (B, C) by a 2x3 color matrix

$$\begin{pmatrix} \Delta_B \\ \Delta_C \end{pmatrix} = \begin{pmatrix} b_1 & b_2 & b_3 \\ c_1 & c_2 & c_3 \end{pmatrix} \begin{pmatrix} (L_t - L_b)/L_b \\ (M_t - M_b)/M_b \\ (S_t - S_b)/S_b \end{pmatrix}. \quad (3)$$

The right-hand side column vector holds the Weber fractions in cone excitations, i.e. the threshold (subscript t) increment divided by the background value (subscript b).

Post-receptoral contrast

In the post-receptoral contrast model, the cone signals for the background and the threshold increment are first converted into cone 'opponent' channels

$$\begin{pmatrix} B \\ C \end{pmatrix} = \begin{pmatrix} b_1 & b_2 & b_3 \\ c_1 & c_2 & c_3 \end{pmatrix} \begin{pmatrix} L \\ M \\ S \end{pmatrix} \quad (4)$$

after which the contrast signals are constructed

$$\Delta_B = (B_t - B_b)/B_b \quad (5a)$$

$$\Delta_C = (C_t - C_b)/C_b \quad (5b)$$

Parameter optimization

Optimization of the model parameters is performed by minimizing the residual sum of squares (RSS) of differences between model (eq.(1)) and data

$$RSS = \sum_{j=1}^n (signal_j - 1)^2 \quad (6)$$

with j running over the data set (n is the number of data points). Equation (6) implies that in the case of a perfect model, all detection signals would equal 1. This is convenient because the value of 1 is then associated with the threshold visibility, and values larger or smaller than 1 indicate above or below visibility threshold, respectively.

We report model errors in terms of RSS and in terms of RMSE (root mean square error) and AIC (Akaike Information Criterion [6]). RMSE is the square root of RSS/n . For AIC we use the formula with sample size correction as detailed in [2]. Both RMSE and AIC are derived from RSS, but we prefer AIC since it includes a penalty for the number of free model parameters and provides a means to calculate relative likelihood for a set of models.

Results

Average observer

Table 2 and Figure 3 capture the results of the model optimizations on the data averaged across observers. We show results for estimations on the separate models (top panels in Fig. 3) and the models on the pooled dataset (bottom panels in Fig. 3). As Table 2 shows, model errors in terms of RSS and RMSE are smaller for the post-receptoral contrast model. This holds for the model estimations on the separate datasets as well as on the pooled datasets. The same conclusion is reached when analyzing the data in terms of Akaike's Information Criterion (AIC). AIC describes the information loss in a model of data. The smaller the loss, the more likely the model is approaching the true model underlying the dataset. For example, the AIC values for the pooled dataset are -732 and -763 for the cone contrast and post-receptoral contrast models, respectively. As a rule of thumb, a difference in these values larger than 2 indicates a significant difference in model likelihood. With a difference of 29 units in this case, this points to a very high difference in probability, in favor of the post-receptoral model (the lower the AIC value, the better). The table also shows the relative likelihood of the models, computed as $\exp(0.5*(AIC_{\min}-AIC_i))$ with AIC_{\min} the minimum AIC value from the models being compared. When post-receptoral contrast is considered as having a (relative) probability of 1, the related cone contrast models only have probabilities in the order of 10^{-5} to 10^{-7} . In all, our earlier finding on the Vogels & Lambooi [1] dataset is reconfirmed on the Xu *et al.* [4] dataset.

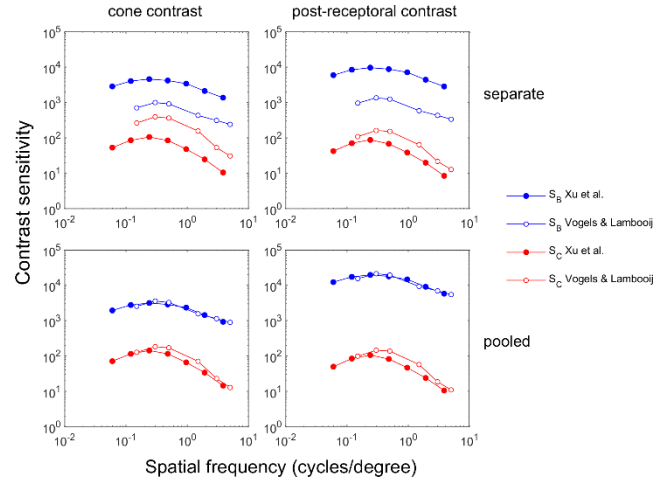


Figure 3: Chromatic contrast sensitivity (S_B and S_C in eq.(1)) estimated with the cone contrast model (left) and post-receptoral contrast model (right) for the average observer. The model parameters were estimated either on the separate data sets (top panels) or on the pooled data (bottom panels). Data points are connected for clarity. See Table 2 also.

The contrast sensitivity graphs shown in Fig.3, obtained for the average observer data, show the typical shape with the leftmost data points lowered. As explained in previous papers [2,5] this is related to the fact that at the lowest spatial frequencies, the number of visible cycles in the fixed stimulus size (limited by the physical dimensions of the stimulus display) is so small that they determine the threshold. They require a higher threshold contrast, hence a lower sensitivity. For higher spatial frequencies, the number of visible cycles is higher and threshold contrast is then determined by spatial frequency. For the separate model fits, a clear difference in absolute value of the contrast sensitivity is noticed. Also, the peak sensitivity for the Xu *et al.* [4] dataset is shifted somewhat to a lower spatial frequency (this is also the case for the pooled dataset). It is related to the fact that the observers' viewing distance in the Xu *et al.* [4] experiment was half that in Vogels & Lambooij [1], while the physical stimulus size was comparable, and therefore the number of cycles was higher, as shown in Fig. 4.

Table 2: Datasets and estimated parameters. n is number of data points, averaged across observers. CC=cone contrast, PR=post-receptoral contrast. pars=number of free model parameters. $b_1..c_3$ refer to the elements of the 2×3 color matrix in eqns.(2-3). $mink$ =minkowski coefficient in eq. (1). RSS=residual sum of squares (eq.(6)). RMSE=root mean square error. AIC_c =Akaike Information Criterion corrected for small sample size.

Dataset	n	model	pars	color matrix						mink	RSS	RMSE	AIC_c	AIC relative likelihood
				b_1	b_2	b_3	c_1	c_2	c_3					
Vogels & Lambooij	72	CC	19	0.730	-0.413	-0.0054	5.830	3.059	0.191	2.27	1.06	0.121	-251	5.5E-05
		PR	19	0.750	-0.013	-0.017	0.562	0.284	4.233	2.06	0.81	0.106	-271	1
Xu et al.	210	CC	21	-0.169	0.055	0.0001	3.665	1.277	0.705	1.63	14.56	0.263	-514	1.6E-06
		PR	21	0.407	0.196	-0.011	0.204	-0.187	0.620	1.41	13.11	0.250	-536	1
Pooled	282	CC	33	-0.275	0.069	0.001	4.046	1.814	0.506	1.83	16.10	0.239	-732	1.9E-07
		PR	33	0.333	0.215	-0.011	0.063	-0.030	0.234	1.60	14.42	0.226	-763	1

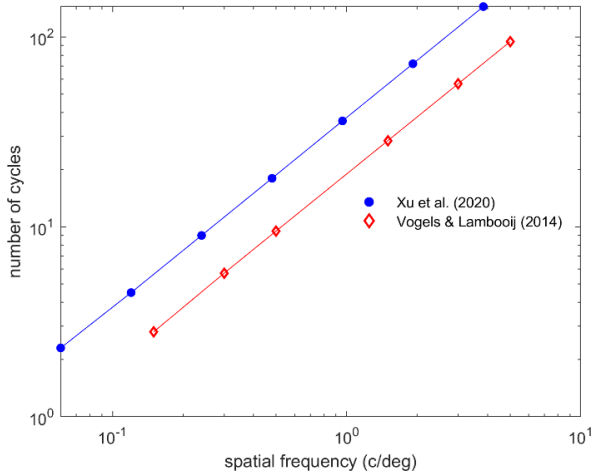


Figure 4: Number of visible cycles in the stimulus area for the different spatial frequencies used in the two studies. The difference in number of cycles is explained by the different viewing distances, while physical stimulus area was the same.

Individual observer

Here we show results of the parameter estimations on the individual observer data. As an example, in Figure 5 the root mean square values (RMSE) are plotted for the data of each participant in the Vogels & Lambooiij [1] experiment. Figure 6 does the same for the participants in the Xu *et al.* [4] experiment.

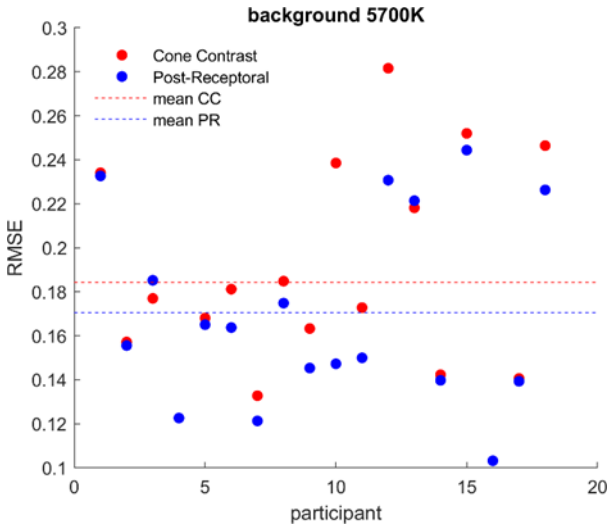


Figure 5: Root mean square error (RMSE) for each participant, for the two contrast models. Background 5700K in the Vogels & Lambooiij [1] dataset. The horizontal dashed lines indicate the mean RMSE values for the contrast models, averaged across the individual observer estimations.

The examples show the conditions with the most comparable background color, 5700 K in [1] and 6500 K in [4], other conditions show similar results. The dashed horizontal lines in the figures represent the mean RMSE values when averaged over the RMSE values obtained for the individual participant data. Both figures show that the mean value for the post-receptorial model is lower than that of the cone contrast model. To test the statistical significance of this difference we applied a paired t-test on the distribution of RMSE

values (Table 3). For all background conditions we find a significant difference at the 95% confidence level ($p < 0.05$ in the last column of Table 3) between the mean RMSE values of the cone contrast and the post-receptorial contrast model. Note that the mean RMSE values for the Xu *et al.* [4] study are higher than in Vogels & Lambooiij [1]. This is explained by the fact that in the former more spatial frequencies and color modulation directions are measured (see Table 1). For one background color, there are $6 \times 4 = 24$ datapoints in Vogels & Lambooiij [1], and $7 \times 6 = 42$ datapoints in Xu *et al.* [4]. Interestingly, both studies show variations between individual participants that range about a factor of 2-3 in terms of RMSE (or a factor of 5 in terms of RSS). What exactly lies underneath these variations is not known, but at least part of it may reflect individual differences in chromatic response of color normal observers, as can be quantified by individual color matching functions [7]. In Table 4 we show the analysis based on AIC values. The mean AIC values reported were first calculated on the individual observer data and then averaged. Again, the relative likelihood is strongly in favor of the post-receptorial contrast model.

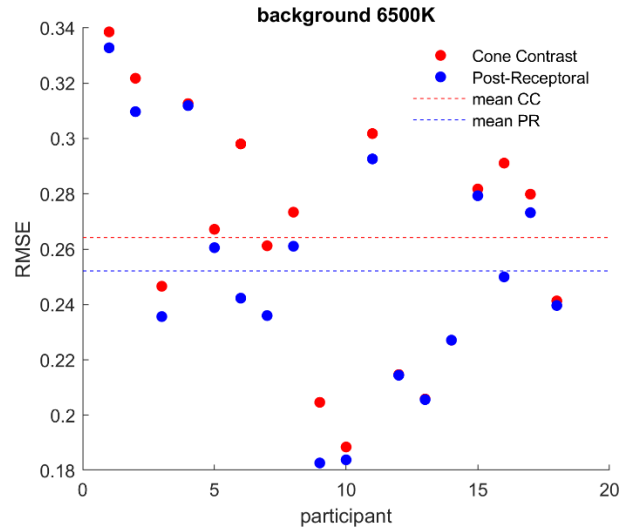


Figure 6: Root mean square error (RMSE) for each participant, for the two contrast models. Background 6500K in the Xu *et al.* [4] dataset. The horizontal dashed lines indicate the mean RMSE values for the contrast models, averaged across the individual observer estimations.

Table 3: Mean RMSE values for the model estimations on individual observer data. CC=cone contrast, PR=post-receptorial contrast. The last column shows the p value on a paired t-test for testing significant difference in the mean RMSE values of the two contrast models.

Dataset	Back-ground	Mean RMSE		p on paired t-test
		CC	PR	
Vogels & Lambooiij	2600 K	0.180	0.173	0.034
	3800 K	0.187	0.172	0.033
	5700 K	0.184	0.171	0.024
Xu et al.	6500 K	0.257	0.253	0.002
	green	0.280	0.270	0.025
	red	0.243	0.235	0.035
	blue	0.236	0.219	0.019
	yellow	0.236	0.224	0.009

Table 4: Mean AIC values for the model estimations on individual observer data. Last two columns show the relative likelihood of the two models.

Dataset	Back-ground	Mean AIC _c		Relative likelihood	
		CC	PR	CC	PR
Vogels & Lambooij	2600 K	-277.1	-283.2	4.7E-02	1
	3800 K	-274.7	-289.0	7.9E-04	1
	5700 K	-275.2	-285.6	5.5E-03	1
Xu et al.	6500 K	-852.6	-874.1	2.1E-05	1
	green	-831.4	-846.4	5.5E-04	1
	red	-891.9	-904.5	1.8E-03	1
	blue	-900.8	-933.7	7.2E-08	1
	yellow	-908.1	-928.4	3.9E-05	1

Cone contrast with nonlinear background normalization

Our results reconfirm, both on the average observer data and the individual observer, that the cone contrast model can be improved upon by processing contrast at the opponent color level. But what is it that makes this post-receptoral contrast model a better descriptor of the data? How is it different from the cone contrast model? To answer that, we looked in more detail into the contrast term of the post-receptoral model. For example, the term $B_t - B_b$ in the nominator of eq.(5a) can be rewritten as

$$\begin{aligned}
 B_t - B_b &= b_1 L_t + b_2 M_t + b_3 S_t - \\
 &\quad (b_1 L_b + b_2 M_b + b_3 S_b) \\
 &= b_1(L_t - L_b) + b_2(M_t - M_b) + b_3(S_t - S_b)
 \end{aligned} \quad (7)$$

Here we recognize the cone specific increment terms $L_t - L_b$ etc. which are also present in the cone contrast model (eq.(3)). What is different in the two models is how these terms are normalized. In the cone contrast model it is normalized by the background value in the same cone type, whereas in the post-receptoral model it is normalized by a mixture of the background values from different cone types (as set by the color matrix in eq.(4)). Apparently, normalization by the linear background value in the same cone type is suboptimal. This invited the idea to normalize the increment terms in the cone contrast model with the background value in a nonlinear fashion:

$$\begin{pmatrix} \Delta_B \\ \Delta_C \end{pmatrix} = \begin{pmatrix} b_1 & b_2 & b_3 \\ c_1 & c_2 & c_3 \end{pmatrix} \begin{pmatrix} (L_t - L_b)/L_b^k \\ (M_t - M_b)/M_b^k \\ (S_t - S_b)/S_b^k \end{pmatrix} \quad (8)$$

in which the background cone excitations are raised to the power of k . A consequence of this is that for the different background luminances in the Xu *et al.* [4] study, the absolute level of the cone excitations is no longer canceled out as in a linear Weber fraction. Also, different luminance levels lead to different retinal illuminance levels because of a change in pupil size. To test the performance of the model in eq.(8), we therefore first corrected the cone excitation values with a factor that takes into account the conversion from corneal luminance to retinal illuminance, as shown in Table 5. The correction factor (last column in Table 5) is the ratio of the retinal illuminance to luminance. Retinal illumination (in trolands) is calculated as the product of luminance (L) and pupil area (in mm^2)

$$T = L \frac{\pi}{4} d^2 \quad (9)$$

with d pupil diameter in mm. The pupil diameter was estimated with the Watson & Yellot [8] formula, entering binocular viewing, age 30, and the proper stimulus dimensions in degrees visual angle for the two studies. Using the corrected cone excitations as input for the model in eq.(8) we find optimized weighting factors $k=0.56$ for the Vogels & Lambooij [1] study, and 0.89 for the Xu *et al.* [4] study. Table 6 summarizes the results in terms of RSS (residual sum of squares) and AIC (Akaike's Information Criterion). The latter accounts for the number of free parameters in the models [6]. Generally, the lower the AIC value, the better the model represents the data. For comparison, the RMSE values for the cone contrast and post-receptoral contrast models in Table 6 are copied from Table 2. When comparing the RMSE values, the cone contrast model with linear cone contrast in the same order of magnitude as the post-receptoral contrast model. However, the AIC values for the post-receptoral model are still some 5 units lower, indicating a higher likelihood for that model. The relative likelihood of the cone contrast model with non-linear background scaling is calculated as $\exp(0.5 \cdot \Delta \text{AIC}) = \exp(0.5 \cdot -5) = 0.082$. In other words, the post-receptoral contrast model is about 12 times as likely to be the model that best minimizes the loss of information in describing the dataset.

Table 5: Conversion factor (last column) to convert from background luminance to retinal trolands, using pupil size (d) estimated by the Watson & Yellot [8] formula.

Dataset	Adapting backgr	L (cd/m ²)	d (mm)	T (Td)	factor T/L
Vogels & Lambooij [1]	2600 K	108	3.42	992.1	9.19
	3800 K	108	3.42	992.1	9.19
	5700 K	108	3.42	992.1	9.19
Xu et al. [4]	6500 K	72	3.06	529.5	7.35
	green	24	3.50	230.9	9.62
	red	14.1	3.76	156.6	11.10
	blue	8.8	4.00	110.6	12.57
	yellow	50	3.20	402.1	8.04

Table 6: Model performance in terms of RMSE and AIC for the two datasets and different contrast models.

dataset	Cone contrast		Post-receptoral contrast		Cone contrast nonlin backgr	
	RMSE	AICc	RMSE	AICc	RMSE	AICc
Vogels & Lambooij	0.121	-251.1	0.106	-270.5	0.107	-265.9
Xu et al.	0.263	-513.5	0.250	-535.6	0.251	-530.6

Conclusion

Based on an analysis of the datasets from the Vogels & Lambooij [1] and Xu *et al.* [4] studies on chromatic contrast visibility, we reconfirm our previously reported finding that a post-receptoral contrast model outperforms the cone contrast model. This was concluded after considering both the individual and average observer data. The cone contrast model however can be improved when applying a nonlinear background weighting (per cone type) but is still outperformed by the post-receptoral model.

Discussion

Chromatic contrast sensitivity models deal with the processing of spatial color information and therefore are relevant for topics like image quality and uniform color space. Having an accurate model is important, as it can help to better predict the visibility of chromatic distortions. We have used different metrics for model accuracy in this paper, all based on the residual sum of squares (RSS). Model comparison using the AIC statistic clearly indicates higher likelihood for the post-receptor contrast model, both on the separate and pooled datasets and both for the average and individual observer data. In terms of RSS, an improvement of almost similar size to the cone contrast model can be achieved when applying a nonlinear background normalization to the cone increment threshold. Such a nonlinear weighting of the increment threshold is well known in visual science. The De Vries-Rose law [9,10] for instance uses a square root on the background intensity, which corresponds to a slope of 0.5 in a log-log plot of threshold increment versus background intensity. This law applies to low light levels where increment thresholds are determined by quantal fluctuations in the light. At higher light levels, linear weighting in Weber's law (slope 1 in log-log plot) applies. The nonlinear weight factors of 0.56 and 0.89 that we determined for our datasets are in between 0.5 and 1 and might thus be interpreted as relating to light levels (within each cone type) in the transition area between the De Vries-Rose and Weber's law [e.g. 11,12]. The fact that we found a higher value (0.89 vs 0.56) for the Xu *et al.* [4] dataset might be explained by the shorter viewing distance (0.5 vs 1 m), leading to a larger retinal field of view of the LCD monitor. So, in the Xu *et al.* [4] experiment the spatially integrated retinal illumination was higher, which may position it closer to the Weber region than the De Vries-Rose region.

With respect to the optimization procedures (performed in Excel and Matlab), it would make sense to use a template function as in the studies by Mantiuk *et al.* [3] and Wuerger *et al.* [13] to fit the shape of the contrast sensitivity curve, as it can reduce the number of free parameters, in particular for the model fits on pooled datasets with differing values for the measured spatial frequencies. In those studies, the pooled data represent widely varying experimental conditions like luminance level and stimulus size, which may partly explain why the Mantiuk *et al.* [3] study did not find a higher performance of the post-receptor contrast model.

It will require more work however to draw final conclusions regarding model differentiation. More data might not be the solution here per se, perhaps insights from physiology can already put the models in better context. For example, we calculate model responses based on cone inputs, but we do nothing with the fact that cones receive feedback signals from horizontal cells which interconnect them, thereby modulating the cone outputs (e.g. [14,15]).

References

- [1] I. Vogels & M. Lambooi, "Visibility of spatial chromatic contrast for lighting applications", in *Experiencing Light 2014: International conference on the effects of light on wellbeing*, Eindhoven, The Netherlands, 2014.
- [2] M. Lucassen, M. Lambooi, D. Sekulovski & I. Vogels, "Spatio-chromatic sensitivity explained by post-receptor contrast", *J. Vision*, 18(5):13, 2018.
- [3] R. Mantiuk, M. Kim, M. Ashraf, Q. Xu, R. Luo, J. Martinovic & S. Wuerger, "Practical color contrast sensitivity functions for luminance levels up to 10 000 cd/m²", in *Twenty Eighth Color and Imaging Conference*, Society for Imaging Science and Technology, 2020.
- [4] Q. Xu., M.R. Luo & D. Sekulovski (2020, September). Investigation of Spatial Chromatic Contrast around 5 Colour Centres. In *London Imaging Meeting (Vol. 2020, No. 1, pp. 1-4)*. Society for Imaging Science and Technology.
- [5] Q. Xu, S. Westland, M. Lucassen, D. Sekulovski, S. Wuerger, R. Mantiuk & R. Luo, "Are Spatial Chromatic Contrast Sensitivity Band-pass or Lowpass Functions?", in *Twenty Eighth Color and Imaging Conference*, Society for Imaging Science and Technology, 2020.
- [6] H. Akaike, "A new look at the statistical model identification", *IEEE Transactions on Automatic Control*, 19, 716–723, 1974.
- [7] Y. Asano, M. Fairchild & L. Blondé, "Individual colorimetric observer model", *PloS one*, 11(2), e0145671, 2016.
- [8] A. Watson & J. Yellott, "A unified formula for light-adapted pupil size", *J. Vision*, 12(10):12, 2012.
- [9] H. De Vries (1943). The quantum character of light and its bearing upon threshold of vision, the differential sensitivity and visual acuity of the eye. *Physica*, 10(7), 553-564.
- [10] A. Rose (1948). The sensitivity performance of the human eye on an absolute scale. *JOSA*, 38(2), 196-208.
- [11] G. Van der Horst & M. Bouman, "Spatio-temporal chromaticity discrimination", *J. Opt. Soc. Am.*, 59, 1482-1488, 1969.
- [12] M. Díez-Ajenjo & P. Capilla, "Spatio-temporal contrast sensitivity in the cardinal directions of the colour space. A review", *J. Optom.*, 3(1), 2-19, 2010.
- [13] S. Wuerger, M. Ashraf, M. Kim, J. Martinovic, M. Pérez-Ortiz & R. Mantiuk, "Spatio-chromatic contrast sensitivity under mesopic and photopic light levels", *J. Vision*, 20(4), 23-23, 2020.
- [14] Chapot, C. A., Euler, T., & Schubert, T. (2017). How do horizontal cells 'talk' to cone photoreceptors? Different levels of complexity at the cone–horizontal cell synapse. *The Journal of physiology*, 595(16), 5495-5506.
- [15] Kamar, S., Howlett, M. H., & Kamermans, M. (2019). Silent-substitution stimuli silence the light responses of cones but not their output. *Journal of vision*, 19(5), 14-14.

Author Biography

Marcel Lucassen, Dragan Sekulovski and Marc Lambooi are scientists at the Lighting Applications group within Signify Research. Their work focuses on the understanding and modeling of perceptual phenomena related to light, lighting and color. Qiang Xu is a PhD student supervised by Prof. Ming Ronnier Luo at the Colour Engineering Lab, College of Optical Science and Engineering, Zhejiang University.